THE JOURNAL OF PHYSICAL CHEMISTRY C

Article

pubs.acs.org/JPCC

Grain Boundary Effect on Electrical Transport Properties of Graphene

Hengji Zhang,[†,‡] Geunsik Lee,[†,∥] Cheng Gong,[†] Luigi Colombo,[§] and Kyeongjae Cho*[,†,‡]

[†]Department of Materials Science and Engineering, and [‡]Department of Physics, The University of Texas at Dallas, Richardson, Texas 75080, United States

[§]Texas Instruments Incorporated, Dallas, Texas 75243, United States

ABSTRACT: The presence of grain boundary affects the mechanical strength, thermal dissipation, and charge transport of polycrystalline graphene flakes. There is still a debate on whether the electronic transmission is severely degraded by the grain boundary, especially between simulations and experiments. To address this issue, we performed electrical transport simulations based on π-orbital tight-binding Hamiltonian. Our results show that the intrinsic grain boundary is almost transparent for the carrier transport, but extrinsic chemical species (e.g., oxygen, hydroxyl) favor the adsorption on interdomain sites and increase the scattering substantially at the boundary region. The experiment, which shows degraded carrier transport due to grain boundary, can be plausibly explained with our theoretical results. To minimize the extrinsic effects of grain boundaries, we suggest doing electrical measurements under ultrahigh-vacuum condition after thermal annealing or applying pulsed current for desorbing the adsobates.

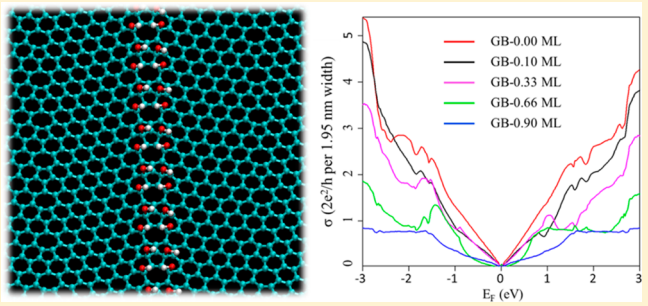

1. INTRODUCTION

Graphene, which is a monolayer graphite, has been considered to be one of the next generation materials in the semiconductor industry due to its appealing electronic,[1] thermal,[2−4] and mechanical properties.[5,6] It was first produced by mechanical exfoliation from highly oriented pyrolytic graphite (HOPG) in 2004.[1] However, HOPG possesses various kinds of extended defects such as monatomic steps, trenches, grain boundaries (GBs), etc.[7] Identification of the structural details of these defects has been done via scanning tunneling microscopy (STM),[8−11] where graphite has been used as a standard substrate in STM experiments for over 25 years. Due to the electronic coupling between the topmost layer and the graphite substrate underneath, the top layer graphene usually exhibits a triangular lattice with 0.246 nm periodicity. There has been also the observation of the honeycomb lattice, where different origins have been suggested such as multiple tip effect,[12] lateral translation,[13] and weakened coupling between the top two layers due to the lift-up of the surface layer by the STM tip.[14] On the basis of the simultaneous observation of both triangular and honeycomb lattices, it was claimed that grain boundaries exist between two domains.[13] The super periodicity of 1−10 nm, i.e., superlattice, has been evidenced in atomic-scale images, and the most probable reason is a rotation of the topmost layer on the graphite substrate.[15] Such a superlattice extends hundreds of nanometers until interfacing with a neighboring domain of a different periodicity or orientation.[8,9] The atomic structure of the grain boundary was first proposed in 2002.[10] From this study, the boundary consists of pentagon and heptagon rings connected together. Such defects are expected to create localized electronic states, resulting in the bright strand in the STM image. Such localized states extending up to 4 nm away from a GB were observed in a recent experiment.[11]

In order to facilitate graphene in the semiconductor industry based on carbon, synthesis of a large-size graphene flake is required. Atomically flat graphene sheets of micrometer scale in lateral size can be obtained on SiC surface by sublimating Si atoms.[16] However, the electrical quality is dependent on the domain size after graphitization. For example, the C-terminated surface of SiC has a carrier mobility as high as 5000 $cm^2/(V{\cdot}s)$, which is about 5 times that of the Si-terminated one.[17] Accordingly, graphene grown on the C face has domain sizes more than 3 times larger than those grown on the Si face.[18] Consistently, the carrier mobility was improved by 2 or 3 times when the terrace size of the Si face was enlarged by 5−8 times through graphitization under Ar gas annealing.[19] Meanwhile, it is not likely that the step edges have a major negative impact on the carrier mobility, based on the measurement that the carrier mobility parallel or perpendicular to the edges is not significantly different.[17,19] Hence, it has been claimed that the continuous graphene film is formed over the steps.[20] Therefore, the number of domain boundaries other than terrace edges mainly affects the carrier mobility. Along with these indications of the presence of grain boundaries, it has been shown that two neighboring graphene regions with the same height and separated by a narrow intervening $6\sqrt{3}$ domain have nonequivalent translations.[21] This indicates that the GB is likely to be formed. Also the existence of the GB has been claimed in the STM, transmission electron microscopy (TEM),

Received: November 21, 2013
Revised: January 7, 2014
Published: January 9, 2014

   dx.doi.org/10.1021/jp411464w | J. Phys. Chem. C 2014, 118, 2338−2343

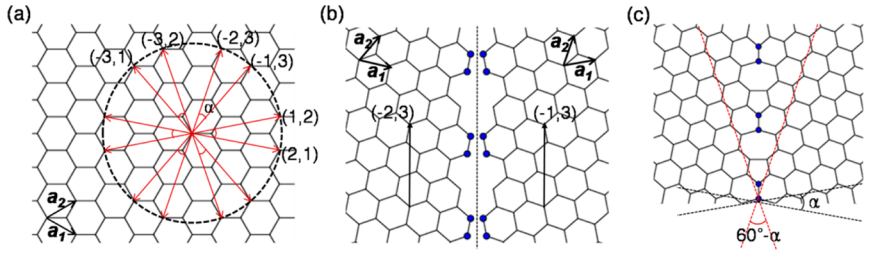

Figure 1. Schematic illustration of GB model structure construction. (a) Twelve chirality vectors of the same length $\sqrt{7}a$ with a = 0.246 nm are illustrated in terms of $ma_1 + na_2 = (m, n)$. Each vector can be used to define the edge of a semi-infinite graphene sheet with the periodicity equal to the length. (b) Two semi-infinite graphene sheets before forming bonds between their edges. Here the chirality vectors $(-1, 3)$ and $(-2, 3)$ are used to define the edges. The filled circles indicate overlapping carbon atoms upon forming the GB, where half of such carbon atoms should be removed. (c) The constructed GB with pentagon−heptagon defects along the boundary. The indicated tilted angle corresponds to α = 21.8°, which is consistent with the experiments (ref 10).

and optical microscopy measurements.[22−24] In recent years, chemical vapor deposition (CVD) of hydrocarbon molecules on copper foils provides the community an economical way of producing large-area single-layer graphene with sparse distribution of multilayers.[25] The predominant defect in these CVD graphene films is the grain boundary that is formed when neighboring nucleation sites expand and coalesce. A number of experimental efforts are devoted to decreasing the domain densities with fewer boundaries, which is expected to be an effective means to enhance the electrical transport property of CVD graphene.[26] These efforts encompass a range of directions involving graphene production temperatures, methane/hydrogen partial pressures, copper foil surface crystallinity, and nucleation site density.

Grain boundary is therefore one of the main problems to be tackled to realize high-speed graphene-based devices. It is likely to degrade thermal[27,28] and electron transport significantly. In experiments, contradictory results emerge about whether the presence of grain boundary degrades the charge transport across it. Yu et al. showed an increased resistance across grain boundary,[29] whereas Huang et al. declared that grain boundaries are not particularly resistive.[23] The recent experiment also shows that the interdomain connectivity of GB can affect electrical conductance.[30] In theoretical works, studies on the electronic band structure and the stability in the presence of the grain boundary have been reported recently,[31] which have shown that the Dirac point is not destroyed. Moreover, it is predicted that electron transport across GB would not be degraded that much.[32] The discrepancy in experimental and theoretical works highlights the significance of understanding the impact of grain boundary on the interdomain electronic transport. Recently, several theoretical papers have investigated possible factors that might degrade charge transport across grain boundary. For example, the low transport mobility could be due to the GB dislocation density,[33] the disorder of GB,[34] and the average grain size and interdomain connectivity of GB.[35] As GB is also a favorable site to adsorb extrinsic impurities (e.g., oxygen, hydroxyl, hydrogen, etc.) in experimental synthesis or measurement condition,[24] in this work we have investigated the GB effects on the electronic structure and how the adsorbed extrinsic impurities on GB sites affect the charge carrier transport of polycrystalline graphene.

2. THEORETICAL METHODS

2.1. Charge-Transport Model. The Hamiltonian of graphene, H, is determined by the π-orbital tight-binding method (π-TB), and the electron hopping parameter, t = −2.7 eV, is used to reproduce π band energy dispersion for graphene. The charge-transport property is calculated based on the nonequilibrium Green's function (NEGF) method.[36] The devices have source and drain electrodes, which are semi-infinite pristine graphene. The channel is in the mid region, where grain boundaries exist to scatter charge transport. In the NEGF method, the retarded Green's function can be expressed as

$$G = [E - H - \sum_{s} - \sum_{D}]^{-1}$$

where $\sum_s$ and $\sum_D$ are self-energy terms to describe interactions between the channel and the source/drain electrodes, respectively. The energy-dependent electrical conductance can be defined as

$$g = \frac{2e^2}{h} Tr(G\Gamma_s G^{+}\Gamma_D)$$

where $\Gamma_{S(D)} = i[\sum_{s(D)} - \sum^{+}_{s(D)}]$ are the energy-broadening matrices.

2.2. GB Model Structure. The GB model is a periodic arrangement of pentagon−heptagon pairs along the boundary proposed by ref 10. Two domains of an ideal honeycomb lattice along different orientations are combined together with a specific C−C bonding structure which comprises a GB. By adjusting lateral positions of carbon atoms at the GB, the pentagon−heptagon rings can be constructed along the boundary. In order to be energetically favorable, two domains have the same number of edge carbon atoms for a given length along the GB. Otherwise, incommensurateness will cause large strain energy, dangling bonds, or other defects. So, there is a specific misorientation angle between two domains at the favorable GB. To clarify this issue, we introduce chirality vector $\mathbf{W}_p = ma_1 + na_2 = (m, n)$ as in CNT studies. Two graphene sheets are prepared with different $\mathbf{W}_p$ vectors, and the edge is made to be parallel to the $\mathbf{W}_p$ for each of them. When two domains are combined, the original $\mathbf{W}_p$ vector has the meaning of periodic lattice vector along the GB, assuming the same length of the two $\mathbf{W}_p$ vectors. In Figure 1, we illustrate an example of the shortest periodicity along GB. The $\mathbf{W}_p$ indicated by (m, n) in Figure 1a has the length of $\sqrt{7}a$ with a = 0.246 nm. There are 12 such vectors with the same length, represented by the arrows ending at the dotted circle. One can choose two different $\mathbf{W}_p$ vectors arbitrarily, but 60° or its integer multiple angles difference should be avoided as it gives zero misorientation angle due to symmetry. For example, $(-2, 3)$ and $(-1, 3)$ are chosen in Figure 1. With combining two

dx.doi.org/10.1021/jp411464w | J. Phys. Chem. C 2014, 118, 2338−2343

semi-infinite sheets defined by those two vectors, the resulting shape is shown in Figure 1b before forming bonds between two edges. To remove the overlapping carbon atoms, half of them are removed to form the GB. The resulting model structure is shown in Figure 1c. Within one periodic length along GB, there are one pentagon−heptagon pair and one hexagon. The angle of tilted orientation, α in Figure 1, is 21.8°. As shown in ref 30, the GB is perfectly transparent or semiconducting depending on the chiralities of two domains. In this study, only transparent cases are considered to study the degrading effect of GB.

3. RESULTS AND DISCUSSION

3.1. Electronic Bands for Periodic Systems. The GB defects are expected to cause localized electronic states near the boundary. Assuming most part of the system is ideal graphene, we focus on how the GB affects the electronic band structure. First, we consider ideal graphene. For comparison with the GB results later, we choose a supercell with one lattice vector the same as one of the chirality vectors in Figure 1a. As shown in Figure 2a, our previous chirality vector $-2a_1 + 3a_2$ is now one

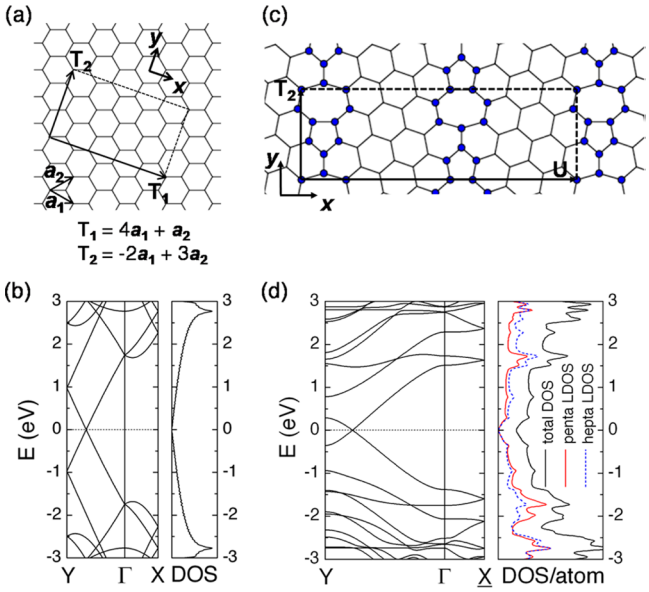

Figure 2. Comparison of electronic band structures with and without GB. (a) Rectangular supercell of ideal graphene with lattice vectors $\mathbf{T}_1 = 4a_1 + a_2$ and $\mathbf{T}_2 = -2a_1 + 3a_2$. $\mathbf{T}_2$ is one of the chirality vectors in Figure 1, and $\mathbf{T}_1$ is the shortest orthogonal vector with integer multiples of a_1 and a_2. (b) Its band structure by the π-TB method, and its density of states (DOS). (c) Periodic unit cell model with the GB. The periodicity requires two GBs of opposite tilt angles in the unit cell. The lattice vector $\mathbf{T}_2$ is the same as that in panel a. (d) Its band structure, shown in the left, and density of states (DOS), shown in the right, are calculated by the π-TB method. Total DOS is shifted up for clarity, and local DOS are projected onto five or seven carbon atoms belonging to pentagon ("penta LDOS") or heptagon ("hepta LDOS") rings.

of primitive lattice vectors of the rectangular cell $(\mathbf{T}_1, \mathbf{T}_2)$, which is along the y-axis. Along the x-axis, the shortest vector $\mathbf{T}_1 = 4a_1 + a_2$ can be obtained by using orthogonal condition. This periodic boundary condition is similar to the case of rolled-up CNT with $\mathbf{T}_2$ being the circumference, but many quantized wave vectors along $\mathbf{T}_2$ can be possible. Hence, it is different from CNT case which allows only the $k = 0$ state for the circumference direction. Under the rectangular supercell in Figure 2a, the Dirac point would be mapped into certain points along the $\Gamma-Y$ direction of the Brillouin zone. As shown in Figure 2b, the band structure calculated by the π-TB method shows that two Dirac points are mapped into $(0, 2\pi/3\mathbf{T}_2)$ and $(0, 4\pi/3\mathbf{T}_2)$. Since there are two ideal graphene domains in the system involving one GB, another chirality vector $-a_1 + 3a_2$ needs to be checked. We confirmed that this also gives the same dispersion as shown in Figure 2b.

For the effect of GB, the periodic unit cells are constructed as shown in Figure 2c. The periodicity requires two GBs of opposite tilt angles in the unit cell. The GB is parallel to the y-axis. The lattice vector along y-axis $\mathbf{T}_2 = -2a_1 + 3a_2$ is the same as that of the previous ideal graphene case, while a different lattice vector $\mathbf{U}$ is used along the x-direction. Its band structure by the same π-TB method is shown in Figure 2d. Overall character of the energy gaps in Figure 2d is similar to that in Figure 2b, i.e., a significant energy gap (>2 eV) along $\Gamma-X$ but metallic bands along the $\Gamma-Y$ direction. Degenerate energy levels at Γ and Y points in Figure 2b are split in Figure 2d. But the Dirac point near the Fermi level remains almost the same, which is consistent with ref 31. This means the GB does not affect the electronic dispersion near the Dirac point. The total and local density of states (DOS) are computed, and the states localized at GB are shown in the right panel of Figure 2d. The shape of total DOS is significantly different from linear shape of ideal graphene, and it is strongly perturbed by GB induced localized states except near the Dirac point. The range of such defect states was measured to be 4 nm,[11] so the strongly perturbed DOS in our result using $|U| = 2$ nm can be understood. The first peak induced by GB defect appears 0.3 eV above or −0.4 eV below the Fermi level. This is well-consistent with STM experiment[11] supporting the validity of the employed GB structure model.

3.2. Electron Transport across the GB. Electron transport across the GB is simulated with the model structure shown in Figure 3a. The periodic boundary condition is imposed along the transverse direction, and 64 k-points sampling along that direction are used to get smooth conductance curves. Figure 3b shows simulated conductance across the GB together with the ballistic conductance for ideal graphene. One can see that the conductance is quite close to the ballistic value (it is a factor of 0.76 at $|E| < 1.5$ eV) although it shows larger decrease at $|E| > 1.5$ eV. From Figure 3c, the local density of states at $|E| < 1.5$ eV remains almost constant along the transport direction and increasing DOS can be seen with approaching the GB. This is also shown in Figure 3d. The increased DOS close to the GB is likely to enhance chemical reactivity with extrinsic defects. Although it decreases the ballistic conductance to a factor of 0.76, this is almost negligible compared to other environmental effects such as charged impurities and ripples which are ascribed to be main sources of mobility drawback. In addition, one can observe the bright stripe near the GB with the energy close to zero in Figure 3c, and this feature also can be seen in Figure 3d. This is reflecting localized states near the Fermi level as observed in the experiment.[11]

The experimentally accessible Fermi level for graphene is quite narrow in typically fabricated devices. The commonly used substrate is SiO_2 with a thickness of 300 nm. A relation between the graphene's Fermi level (E_F) and the gate voltage (V_g) is given by $V_g \sim 1000E_F^2$.[37] Under the variation of V_g from 0 to 50 V, the E_F changes from 0 to 0.22 eV. In this range, we have seen the conductance is decreased less than 1 order by the

dx.doi.org/10.1021/jp411464w | J. Phys. Chem. C 2014, 118, 2338−2343

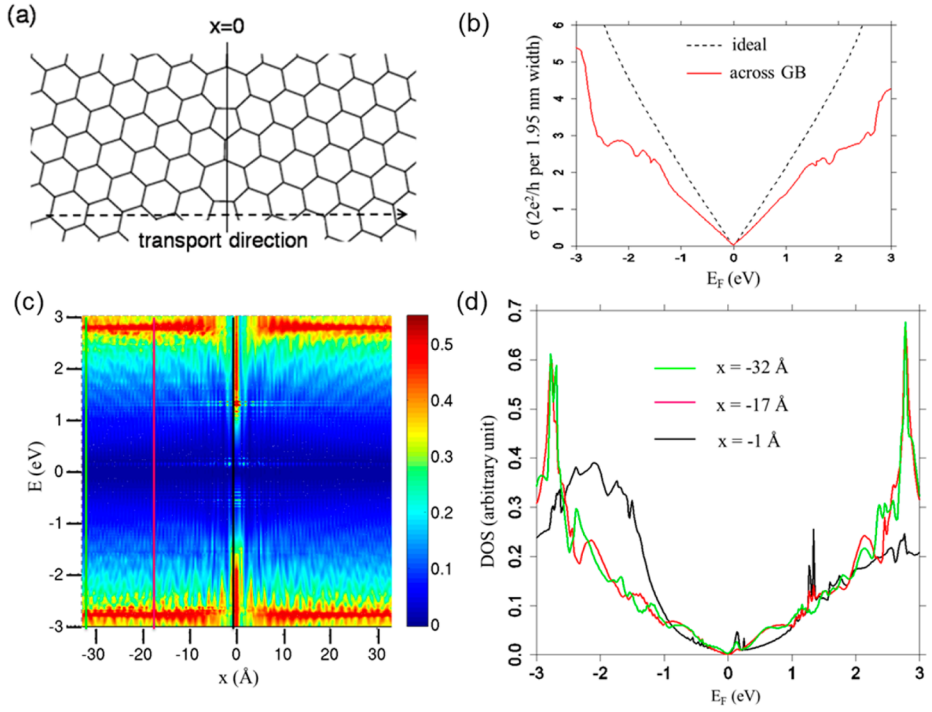

Figure 3. Electron transport across the GB. (a) The channel structure for transport simulation across the GB. (b) The calculated conductance for the GB (red solid line) normalized to 1.95 nm width. Also, the ideal graphene conductance (dashed line) is shown. (c) Spectral local density of states is mapped along the transport direction with averaging over transverse direction. (d) Local density of states for specific positions of $x = -3.2, -1.7, -0.1$ nm. The y-axis scale is the same as the color bar shown in panel c.

Table 1. Chemisorption Energies of H, O, and OH Species at the Atomic Sites of Grain Boundary[a]

	1	2	3	4	5	6	7	bulk site
H	1.42 (1.11)	2.06 (1.66)	1.94 (1.56)	1.73 (1.49)	1.66 (1.31)	1.91 (1.55)	N/A	1.39 (1.00)
O	3.34 (2.50)	3.33 (2.49)	3.45 (2.61)	3.21 (2.16)	3.65 (2.79)	4.45 (3.52)[b]	3.36 (2.54)	2.98 (2.09)
OH	2.00 (1.25)	2.48 (1.80)	2.24 (1.41)	2.09 (1.62)	2.14 (1.47)	2.31 (1.67)	N/A	1.64 (1.18)

[a]The adsorption sites are labeled in the figure below. The top sites are for H or OH, and the bridge sites are for O. Both ab initio results from LDA and GGA (in parentheses) are shown here.

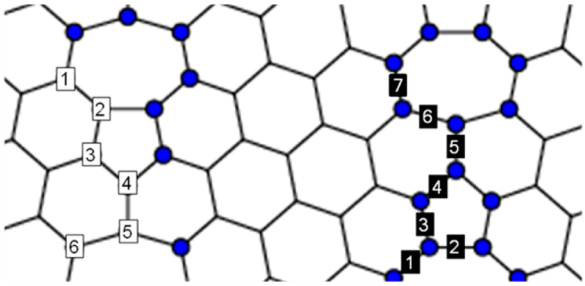

[b]LDA and GGA predict σ-bonded C−O−C structure breaking the underlying C−C bond.

GB. Therefore, the GB itself should not have significant impact on the measured conductance of graphene.

3.3. Extrinsic Effect on Conductance of GB. The carrier mobility of large-size graphene flakes, usually prepared by epitaxial methods, is on the order of 1000 $cm^2/(V{\cdot}s)$,[17,38] which is 1 order lower than that of small flakes. It is said that polycrystalline character is mainly responsible for the mobility degradation in large flakes, assuming similar magnitudes of other environmental effects. The GB is one of the major defects existing in the polycrystalline structure, and our study shows that the intrinsic GB is not the limiting factor at all. Rather the main factor could be the extrinsic effect, which is passivation of the π-orbital at the GB. Since the GB is expected to be chemically reactive toward π-orbital passivation by foreign species, the conductance will be suppressed by π-orbital passivation. According to our ab initio density functional theory (DFT) calculations shown in Table 1, the chemisorption energies of O at the bridge site and H or OH at the top site of the GB are always larger than bulk site adsorptions. The ab initio calculation is done with VASP[39] based on the projector-augmented wave pseudopotential method. We have used local density approximation (LDA) and generalized gradient approximation (GGA) to describe the exchange-correlation functional terms.

The effect of extrinsic π-orbital passivation at the GB has been studied in the following way. For a given GB passivation

dx.doi.org/10.1021/jp411464w | J. Phys. Chem. C 2014, 118, 2338−2343

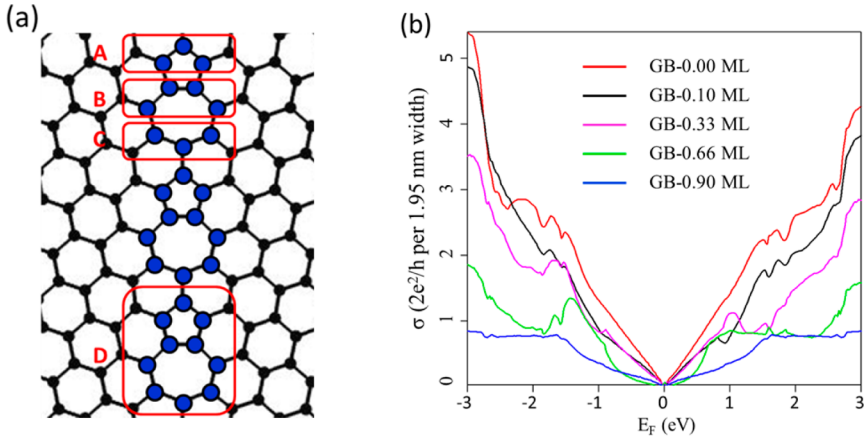

Figure 4. Electrical conductance of GB with extrinsic defects. (a) GB in graphene with the width of 1.95 nm. The extrinsic molecule species are bonded with the carbon atoms (blue) at the GB sites. The red lines that enclose parts A–D represent the basic patterns of π-orbital passivation, which is used to construct the GB with different extrinsic defect concentrations. A–C patterns are used for 0.10 and 0.90 ML, and D is used for 0.33 and 0.66 ML. (b) Electrical conductance for the GB at different extrinsic concentrations. For 0.10 and 0.90 ML, there are three inequivalent patterns (e.g., A–C) that can be used to generate the passivation. An average is taken to obtain the electrical conductance for these two-passivation coverages.

coverage, a corresponding number of π-orbitals belonging to pentagon or heptagon rings are removed according to the basic patterns shown in Figure 4a. With an increased coverage, more broken $\pi-\pi$ bonds occur at the GB sites. Thus, the number of $\pi-\pi$ connection pathways between the left and right regions of GB is narrowed, and the conductance is expected to decrease. Practically, the passivation sites for a given coverage concentration would distribute randomly. In this study, our focus is to understand the evolution of electrical conductance as extrinsic defects increase. With the basic patterns (e.g., A–D) shown in Figure 4a, a wide range of extrinsic defect coverage can be readily constructed to represent the diminished $\pi-\pi$ connection pathways as defect concentration increases.

The main conclusion of Figure 4b is that the conductance of the extrinsic GB can be largely reduced as compared with the intrinsic GB. This may explain that the electrical conductance measured within the graphene grain is several times higher than that for across GB.[29] Also, large graphene flakes, like grown on SiC,[17] exhibit 1 order lower carrier mobility than small mechanically exfoliated samples. Since the most electrical measurements are performed in ambient condition, this low carrier mobility is possibly due to the extrinsic effect rather than the intrinsic GB. Although high-symmetry GB is only considered in this study, the degradation of electrical property due to extrinsic defects should prevalently exist for GB with different intrinsic properties (e.g., symmetry, tilt angles, dislocation densities). Finally, it will be worthwhile to examine electrical behavior after removing extrinsic effects. According to the STM measurements in ultrahigh vacuum, the localized electronic states, caused by intrinsic GB, are visible after heating HOPG at 500 °C.[11] With the similar treatment method, the carrier mobility of graphene with GB could be further enhanced.

4. CONCLUSION

In summary, our theoretical investigation shows that the intrinsic GB is almost transparent to the carrier transport. However, foreign species are shown to favor the adsorption on the boundary sites, resulting in the passivation of the available π-orbital with a degraded electronic transport. Probably, the experimentally observed degradation of the charge transport across the grain boundary in graphene is not caused by the intrinsic grain boundary but the passivated grain boundary by extrinsic contaminants. We suggest experimentalists eliminate the extrinsic effects at GB sites by thermal annealing or pulsed current, with the subsequent electrical measurements of the CVD graphene under ultrahigh-vacuum condition.

AUTHOR INFORMATION

Corresponding Author

*E-mail: kjcho@utdallas.edu.

Present Address

[‖]G.L.: Department of Chemistry, Pohang University of Science and Technology, Pohang 790-784, Korea.

Notes

The authors declare no competing financial interest.

ACKNOWLEDGMENTS

This work is supported by Nano·Material Technology Development Program through the National Research Foundation of Korea (NRF) funded by the Ministry of Science, ICT and Future Planning (2012M3A7B4049888).

REFERENCES

(1) Novoselov, K. S.; Geim, A. K.; Morozov, S. V.; Jiang, D.; Zhang, Y.; Dubonos, S. V.; Grigorieva, I. V.; Firsov, A. A. Electric Field Effect in Atomically Thin Carbon Films. *Science* **2004**, *306*, 666–669.

(2) Balandin, A. A.; Ghosh, S.; Bao, W. Z.; Calizo, I.; Teweldebrhan, D.; Miao, F.; Lau, C. N. Superior Thermal Conductivity of Single-Layer Graphene. *Nano Lett.* **2008**, *8*, 902–907.

(3) Seol, J. H.; Jo, I.; Moore, A. L.; Lindsay, L.; Aitken, Z. H.; Pettes, M. T.; Li, X. S.; Yao, Z.; Huang, R.; Broido, D.; Mingo, N.; Ruoff, R. S.; Shi, L. Two-Dimensional Phonon Transport in Supported Graphene. *Science* **2010**, *328*, 213–216.

(4) Chen, S. S.; Wu, Q. Z.; Mishra, C.; Kang, J. Y.; Zhang, H. J.; Cho, K. J.; Cai, W. W.; Balandin, A. A.; Ruoff, R. S. Thermal Conductivity of Isotopically Modified Graphene. *Nat. Mater.* **2012**, *11*, 203–207.

(5) Lee, C.; Wei, X.; Kysar, J. W.; Hone, J. Measurement of the Elastic Properties and Intrinsic Strength of Monolayer Graphene. *Science* **2008**, *321*, 385–388.

(6) Grantab, R.; Shenoy, V. B.; Ruoff, R. S. Anomalous Strength Characteristics of Tilt Grain Boundaries in Graphene. *Science* **2010**, *330*, 946–948.

(7) Pong, W.-T.; Bendall, J.; Durkan, C. Observation and Investigation of Graphite Superlattice Boundaries by Scanning Tunneling Microscopy. *Surf. Sci.* **2007**, *601*, 498−509.
(8) Albrecht, T. R.; Mizes, H. A.; Nogami, J.; Park, S. I.; Quate, C. F. Observation of Tilt Boundaries in Graphite by Scanning Tunneling Microscopy and Associated Multiple Tip Effects. *Appl. Phys. Lett.* **1988**, *52*, 362−364.
(9) Gan, Y.; Chu, W. Y.; Qiao, L. J. STM Investigation on Interaction between Superstructure and Grain Boundary in Graphite. *Surf. Sci.* **2003**, *539*, 120−128.
(10) Simonis, P.; Goffaux, C.; Thiry, P. A.; Biro, L. P.; Lambin, P.; Meunier, V. STM Study of a Grain Boundary in Graphite. *Surf. Sci.* **2002**, *511*, 319−322.
(11) Cervenka, J.; Flipse, C. F. J. Structural and Electronic Properties of Grain Boundaries in Graphite: Planes of Periodically Distributed Point Defects. *Phys. Rev. B* **2009**, *79*, 195429.
(12) Mizes, H. A.; Park, S.; Harrison, W. A. Multiple-Tip Interpretation of Anomalous Scanning-Tunneling-Microscopy Images of Layered Materials. *Phys. Rev. B* **1987**, *36*, 4491−4494.
(13) Wang, Y. F.; Ye, Y. C.; Wu, K. Simultaneous Observation of the Triangular and Honeycomb Structures on Highly Oriented Pyrolytic Graphite at Room Temperature: An STM Study. *Surf. Sci.* **2006**, *600*, 729−734.
(14) Wong, H. S.; Durkan, C.; Chandrasekhar, N. Tailoring the Local Interaction between Graphene Layers in Graphite at the Atomic Scale and Above Using Scanning Tunneling Microscopy. *ACS Nano* **2009**, *3*, 3455−3462.
(15) Beyer, H.; Muller, M.; Schimmel, T. Monolayers of Graphite Rotated by a Defined Angle: Hexagonal Superstructures by STM. *Appl. Phys. A: Mater. Sci. Process* **1999**, *68*, 163−166.
(16) Berger, C.; Song, Z.; Li, X.; Wu, X.; Brown, N.; Naud, C.; Mayou, D.; Li, T.; Hass, J.; Marchenkov, A. N.; Conrad, E. H.; First, P. N.; de Heer, W. A. Electronic Confinement and Coherence in Patterned Epitaxial Graphene. *Science* **2006**, *312*, 1191−1196.
(17) Kedzierski, J.; Hsu, P.-L.; Healey, P.; Wyatt, P. W.; Keast, C. L.; Sprinkle, M.; Berger, C.; de Heer, W. A. Epitaxial Graphene Transistors on SIC Substrates. *IEEE Trans. Electron Devices* **2008**, *55*, 2078−2085.
(18) Hass, J.; Feng, R.; Li, T.; Li, X.; Zong, Z.; de Heer, W. A.; First, P. N.; Conrad, E. H.; Jeffrey, C. A.; Berger, C. Highly Ordered Graphene for Two Dimensional Electronics. *Appl. Phys. Lett.* **2006**, *89*, 143106.
(19) Emtsev, K. V.; Bostwick, A.; Horn, K.; Jobst, J.; Kellogg, G. L.; Ley, L.; McChesney, J. L.; Ohta, T.; Reshanov, S. A.; Roehrl, J.; et al. Towards Wafer-Size Graphene Layers by Atmospheric Pressure Graphitization of Silicon Carbide. *Nat. Mater.* **2009**, *8*, 203−207.
(20) Seyller, T.; Emtsev, K. V.; Gao, K.; Speck, F.; Ley, L.; Tadich, A.; Broekman, L.; Riley, J. D.; Leckey, R. C. G.; Rader, O.; et al. Structural and Electronic Properties of Graphite Layers Grown on SiC(0001). *Surf. Sci.* **2006**, *600*, 3906−3911.
(21) Poon, S. W.; Chen, W.; Tok, E. S.; Wee, A. T. S. Probing Epitaxial Growth of Graphene on Silicon Carbide by Metal Decoration. *Appl. Phys. Lett.* **2008**, *92*, 104102.
(22) Biedermann, L. B.; Bolen, M. L.; Capano, M. A.; Zemlyanov, D.; Reifenberger, R. G. Insights into Few-Layer Epitaxial Graphene Growth on 4H−SiC(000$\bar{1}$) Substrates from STM Studies. *Phys. Rev. B* **2009**, *79*, 125411.
(23) Huang, P. Y.; Ruiz-Vargas, C. S.; van der Zande, A. M.; Whitney, W. S.; Levendorf, M. P.; Kevek, J. W.; Garg, S.; Alden, J. S.; Hustedt, C. J.; Zhu, Y.; et al. Grains and Grain Boundaries in Single-Layer Graphene Atomic Patchwork Quilts. *Nature* **2011**, *469*, 389−392.
(24) Duong, D. L.; Han, G. H.; Lee, S. M.; Gunes, F.; Kim, E. S.; Kim, S. T.; Kim, H.; Quang Huy, T.; So, K. P.; Yoon, S. J.; et al. Probing Graphene Grain Boundaries with Optical Microscopy. *Nature* **2012**, *490*, 235−239.
(25) Li, X.; Magnuson, C. W.; Venugopal, A.; An, J.; Suk, J. W.; Han, B.; Borysiak, M.; Cai, W.; Velamakanni, A.; Zhu, Y.; et al. Graphene Films with Large Domain Size by a Two-Step Chemical Vapor Deposition Process. *Nano Lett.* **2010**, *10*, 4328−4334.
(26) Hao, Y.; Bharathi, M. S.; Wang, L.; Liu, Y.; Chen, H.; Nie, S.; Wang, X.; Chou, H.; Tan, C.; Fallahazad, B.; et al. The Role of Surface Oxygen in the Growth of Large Single-Crystal Graphene on Copper. *Science* **2013**, *342*, 720−723.
(27) Balandin, A. A. Thermal Properties of Graphene and Nanostructured Carbon Materials. *Nat. Mater.* **2011**, *10*, 569−581.
(28) Nika, D. L.; Balandin, A. A. Two-Dimensional Phonon Transport in Graphene. *J. Phys.: Condens. Matter* **2012**, *24*, 233203.
(29) Yu, Q.; Jauregui, L. A.; Wu, W.; Colby, R.; Tian, J.; Su, Z.; Cao, H.; Liu, Z.; Pandey, D.; Wei, D.; et al. Control and Characterization of Individual Grains and Grain Boundaries in Graphene Grown by Chemical Vapour Deposition. *Nat. Mater.* **2011**, *10*, 443−449.
(30) Tsen, A. W.; Brown, L.; Levendorf, M. P.; Ghahari, F.; Huang, P. Y.; Havener, R. W.; Ruiz-Vargas, C. S.; Muller, D. A.; Kim, P.; Park, J. Tailoring Electrical Transport Across Grain Boundaries in Polycrystalline Graphene. *Science* **2012**, *336*, 1143−1146.
(31) Araujo, J. d. S.; Nunes, R. W. Complex Evolution of the Electronic Structure from Polycrystalline to Monocrystalline Graphene: Generation of a New Dirac Point. *Phys. Rev. B* **2010**, *81*, 073408.
(32) Yazyev, O. V.; Louie, S. G. Electronic Transport in Polycrystalline Graphene. *Nat. Mater.* **2010**, *9*, 806−809.
(33) Gargiulo, F.; Yazyev, O. V. Topological Aspects of Charge-Carrier Transmission across Grain Boundaries in Graphene. *Nano Lett.* **2014**, *14*, 250−254.
(34) Vancso, P.; Mark, G. I.; Lambin, P.; Mayer, A.; Hwang, C.; Biro, L. P. Effect of the Disorder in Graphene Grain Boundaries: a Wave Packet Dynamics Study. *Appl. Surf. Sci.* **2013**, *291*, 58−63.
(35) Van Tuan, D.; Kotakoski, J.; Louvet, T.; Ortmann, F.; Meyer, J. C.; Roche, S. Scaling Properties of Charge Transport in Polycrystalline Graphene. *Nano Lett.* **2013**, *13*, 1730−1735.
(36) Datta, S. *Electronic Transport in Mesoscopic Systems*; Cambridge University Press: Cambridge, U.K., 1995.
(37) Du, X.; Skachko, I.; Barker, A.; Andrei, E. Y. Approaching Ballistic Transport in Suspended Graphene. *Nat. Nanotechnol.* **2008**, *3*, 491−495.
(38) Gu, G.; Nie, S.; Feenstra, R. M.; Devaty, R. P.; Choyke, W. J.; Chan, W. K.; Kane, M. G. Field Effect in Epitaxial Graphene on a Silicon Carbide Substrate. *Appl. Phys. Lett.* **2007**, *90*, 253507.
(39) Kresse, G.; Furthmuller, J. Efficiency of Ab-Initio Total Energy Calculations for Metals and Semiconductors Using a Plane-Wave Basis Set. *Comput. Mater. Sci.* **1996**, *6*, 15−50.